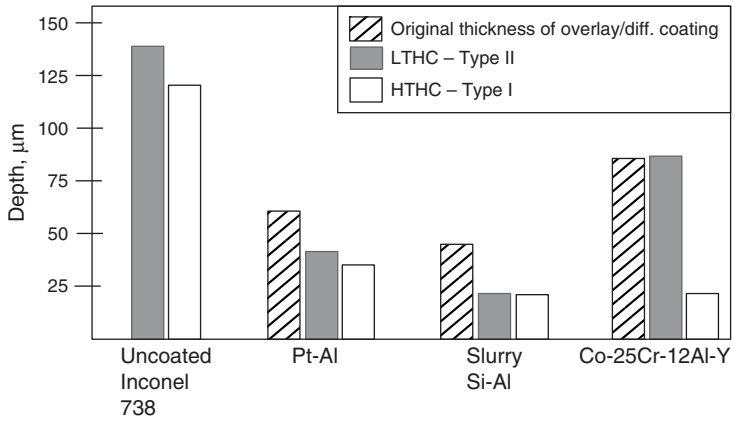

Figure 9.18 Sulphidation attack experiments carried out in a GTE (Tyne RMIC) marine engine for 500 hours under Type I and Type II conditions.
After Meetham, 1986.

9.3 Durability of Thermal Barrier Coating Systems (TBCS) to In-Service Particle Encounters

9.3.1 TBCS Architectures

Two possible thermal barrier coating system (TBCS) architectures are shown in **Figs. 9.19 and 9.20**. Hardware application examples are given in **Fig. 9.21**. TBCS architectures may comprise an inner 'bond coat' and an outer ceramic thermal barrier layer of zirconia (ZrO_2). The latter is single phased. It contains ~8wt-% Y_2O_3 dissolved in solid solution, and its purpose is to stabilise the tetragonal (t) form of zirconia (t-ZrO_2) over the in-service operational temperatures encountered by a given turbine blade. The inner bond coat comprises a hot corrosion-resistant 'diffusion coating' (**Fig. 9.19**) or an 'overlay coating' (**Fig. 9.20**), previously described in **Section 9.2**. One of the most common diffusion coatings for TBCS is Pt-aluminide, whilst several proprietary M-Cr-Al-Y overlays may be chosen (**Table 9.3**). Diffusion coatings are practically limited by diffusion zone growth kinetics to a thickness of ~50µm (and must be kept below 75µm to avoid crack formation – Meetham, 1986); in contrast, M-Cr-Al-Y overlays (having a metal matrix) are more ductile and can be considerably thicker (~100 to 500µm; Hancock, 1986; Boyce 2012; Darolia, 2013). Sandwiched between the two layers is an additional oxide coating (~1 to 3µm thick) which is developed by heating the prior bond/diffusion-coated nickel alloy parts in air at temperatures ~1000°C. This important constituent is termed a 'thermally grown oxide' (TGO) and is typically α-Al_2O_3; it aids adhesion of the outer zirconia layer. Such layers can appreciably thicken (by several micrometres) during operational use, via the diffusion of Al from the 'bond coat' into the TGO. Concerning further aspects of dimensions, the outer t-ZrO_2 coating (**Figs. 9.19 & 9.20**) can be ~100 to 200µm thick, when required for rotating blades, but may be much greater (250 to 500µm) when used for stationary vanes, nozzle guide vanes (NGVs) and combustors (Boyce, 2012; Darolia, 2013). Two methods of application are currently popular: air plasma spraying (APS) *or* reactive electron beam evaporation PVD

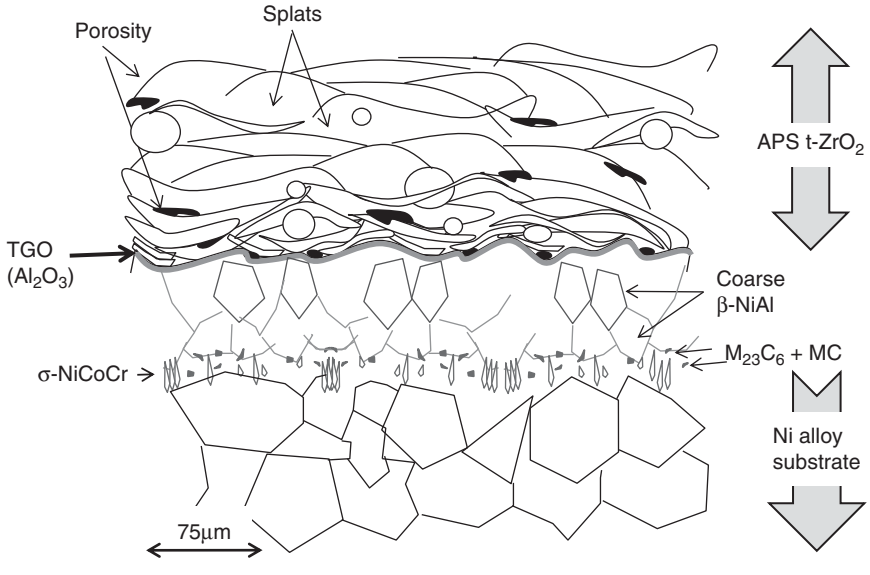

Figure 9.19 Schematic of a thermal barrier coating system (TBCS) comprising: a diffusion aluminide 'bond' coating (either conventional or Pt modified), its thermally grown oxide (TGO) – Al_2O_3 – and a portion of the adjacent APS t-ZrO_2 top coat (next to the TGO) revealing its micro-porosity and splat morphology. The substrate is a polycrystalline Ni-Cr alloy like Inconel 738. It should be noted that a PVD t-ZrO_2 top coat may be used as an alternative to the APS variant shown.

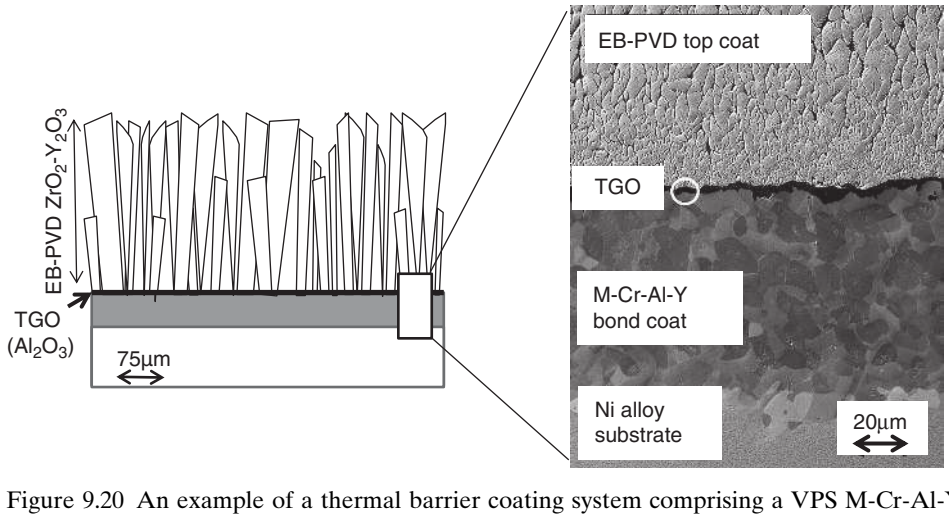

Figure 9.20 An example of a thermal barrier coating system comprising a VPS M-Cr-Al-Y overlay 'bond' coating (thermally homogenised and recrystallised), its thermal growth oxide (TGO) and a portion of the adjacent EB-PVD stabilised t-ZrO_2 top coat (next to the TGO) showing its near equi-axed nature. The substrate is a single-crystal nickel alloy (PWA 1484). Micrograph to right: courtesy of Wolfgang Brau & Springer Science. Used with permission. After Brau, 2009.

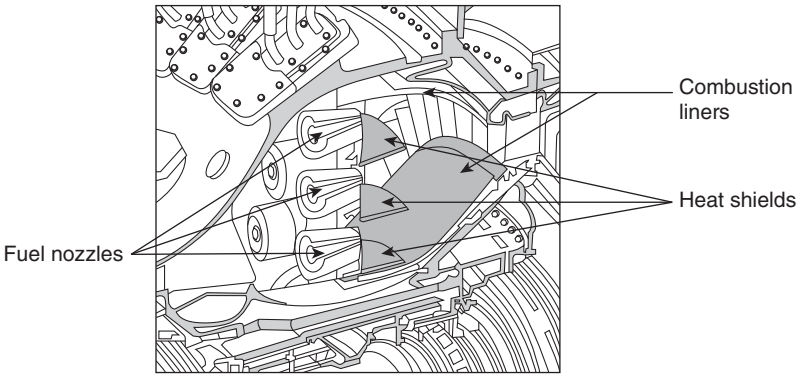

Figure 9.21 Cut-away diagram showing positions of nickel alloy combustion liners and heat shields in a commercial aero-GTE Annular DLE combustor that are protected with thermal barrier coating systems.
After Boyce, 2012. © Elsevier, 2012.

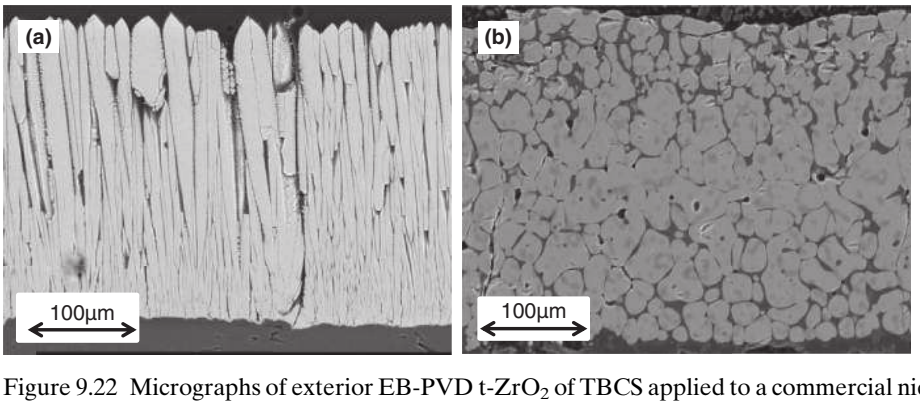

Figure 9.22 Micrographs of exterior EB-PVD t-ZrO_2 of TBCS applied to a commercial nickel alloy: (a) as manufactured; (b) after dissolution by a basic (alkaline) CMAS melt, showing recrystallised ZrO_2 and a new second phase.
After Ndamka, 2013. Courtesy of Dr N. Ndamka, Rolls-Royce, UK.

(EB-PVD) – refer to **Chapter 4**, **Sections 4.11 and 4.14**. The former technology is considered to be cheaper and quicker to apply than the latter, although the surface finish is not as good. This has an impact on heat transfer from air/gases that flow over t-ZrO_2 surfaces in service. Smooth surfaces encourage laminar flow; rough surfaces stimulate turbulent flow. Arguably, the former are more effective in removing heat from the operating environment. Heat transfer through a TBCS is of prime importance. An important property of t-ZrO_2 is that its thermal conductivity (K) is invariant with temperature (Darolia, 2013). Further, it is an order of magnitude lower than that of the adjacent nickel aluminide or M-Cr-Al-Y coating component. The primary role of the of t-ZrO_2 layer is to restrict heat flow. In addition, once heat arrives at the adjacent nickel aluminide or M-Cr-Al-Y coating surfaces, it is quickly dissipated by their greater thermal conductivity – an effect that is augmented further

by the use of internal cooling channels placed within the nickel alloy components (**Fig. 9.4**). This set-up allows any nickel alloy component to be kept at anywhere between 20 to 200°C lower than that of the outer t-ZrO_2 coating surface (Darolia, 2013). Greater details of cooling strategies, including convective air flow, are given by Han and Wright (2007) and Boyce (2012).

Yet a further feature of t-ZrO_2 coatings shown in **Figs. 9.19 and 9.20** is that they show high in-plane strain tolerance. In the case of EB-PVD ZrO_2 variants, this is made possible by the existence of relatively large gaps (>0.5μm) *between* the vertically oriented grain boundaries (**Fig. 9.22a**); these enable lateral expansion and contraction of the ZrO_2 layer without fracture, during regular thermal cycling (this is especially important for aircraft GTEs where endurance to frequent engine stop/starts is required). In contrast, APS-ZrO_2 variants, containing horizontally oriented micro-porosity (located between individual solidified coating 'splats'), provide a similar means of attaining the necessary strain tolerance, although this is arguably less effective than vertical cracked EB-PVD ZrO_2. This disparity has led to efforts to produce a new and improved method of spray deposition: a hybrid technology termed 'plasma spray PVD' or simply 'PS-PVD' (Jordon et al, 2004). Here, very fine (<5μm) ZrO_2-8wt-%Y_2O_3 ceramic source powder is passed through a plasma torch (in partial vacuum) and completely vaporised before being condensed (solidified) on a nickel alloy substrate (coated with a suitable overlay). The substrate is negatively biased during deposition, yielding a process that has a very much improved 'throwing power' compared to APS or VPS techniques. Fortuitously, vertically oriented cracks and quasi-columnar grains develop during solidification, providing PS-PVD ZrO_2 coatings with a strain tolerance similar to that of EB-PVD variants. Moreover, the rates of deposition are higher for PS-PVD ZrO_2 coatings, compared to EB-PVD, which enables a higher manufacturing throughput and (arguably) a lower treatment cost per component. The technology can also be used to apply coatings to non-blade GTE components, like combustor liners, where conventional EB-PVD cannot be used. Given that this is a new technology, the competitiveness of PS-PVD versus APS and VPS has yet to be fully evaluated.

9.3.2 Durability to Particle Chemical (CMAS) and Mechanical (Erosion) Attack

Whether a GTE is land based, as is the case for industrial power generating variants, or is being deployed to provide propulsion for aircraft or ships, its internal working surfaces frequently encounter airborne mineral (ceramic-like) particles. This can result in mechanical (erosion) or chemical (CMAS) attack of nickel alloy surfaces protected with a TBCS. Encounters with mineral particles are amongst the highest in the Middle East, where desert sand is ubiquitous. Here, various mineral particles can be encountered (de Wet et al, 1993), including sand (quartz, α-SiO_2), gypsum ($CaSO_4.2H_2O$), albite ($NaAlSi_3O_8$), calcite ($CaCO_3$), microcline ($KAlSi_3O_8$) and dolomite ($CaMg(CO_3)_2$. Concrete dust from building structures is a further source of

particulates. However, incidents of aircraft straying through volcanic dust clouds (Grindle & Burcham, 2003) in many different parts of the globe have added to concerns regarding GTE operational safety. Particle sizes ~100μm can be easily carried into the turbine section and can cause marked damage. Volcanic ash particles have been grouped under the acronym 'CMAS' to indicate the common ceramic phases they contain – **C**aO, **M**gO, **A**l_2O_3 and **S**iO_2. Depending on the proportions of these phases, the ash may have a basic (alkaline) or acid character. This factor becomes important when GTE hardware surfaces are sufficiently hot (~1250°C) to cause the particles to melt and stick. As is well known, oxide ceramic materials are particularly prone to alkaline attack. This causes t-ZrO_2 to become dissolved, a situation that can be made more pronounced in very high-temperature (~1300–1500°C) laboratory experiments. These show (de Wet et al, 1993; Ndamka, 2014) that t-ZrO_2 can be dissolved and re-precipitated with a spherical morphology (**Fig. 9.22b**). Such effects do *not* take place at similar temperatures when the mix of CMAS oxides has a more acid character. Nonetheless, some deterioration of the t-ZrO_2 takes place (Ndamka, 2014).

One specific source of chemical attack is from molten particles of gypsum ($CaSO_4$) – a major constituent in Middle East sand. In one example, this mineral was observed (Brau, 2011; Brau & Mechnich, 2011) adhered to the surfaces of an EBPVD-ZrO_2-coated blade extracted from the turbine section of one GTE, operated in an aircraft by Lufthansa, after 17,000 hours' service (**Figs. 9.23 to 9.25**). Gypsum has a melting point of 1460°C and when molten, can infiltrate along the vertically oriented columnar grain boundaries of an EB-PVD t-ZrO_2 top coat. This serves to 'bond' or 'weld' together the individual columnar grains (**Fig. 9.25**), making the t-ZrO_2 coating less strain tolerant and more prone to catastrophic fracture during subsequent (i) operational thermal cycling, and/or (ii) erosion by particle bombardment (Ndamka, 2013).

All t-ZrO_2 top coats of any given TBCS have a finite lifetime, making it important to understand their modes of failure. Here, it is worthwhile briefly presenting some important observations regarding their response to bombardment by high-velocity particles which cause eventual deterioration by *erosion*. Diffusion or overlay-coated surfaces without any t-ZrO_2 top coats can also suffer in the same way (Tabakoff, 1999; Nicholls et al, 1999).

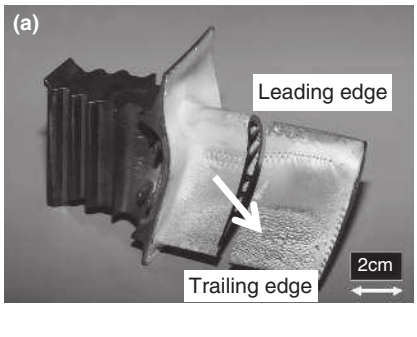

Figure 9.23 Ventilated blade (from a GTE turbine section) retrieved after 17,000 hours' operational use (equivalent to 3000 operational cycles). Note build-up of CMAS deposits towards trailing edge of the pressure face (arrow). Courtesy of Wolfgang Brau, Peter Mechnich and Wiley Publications (J. American Ceramic Society). Used with permission. After Brau & Mechnich (2011).

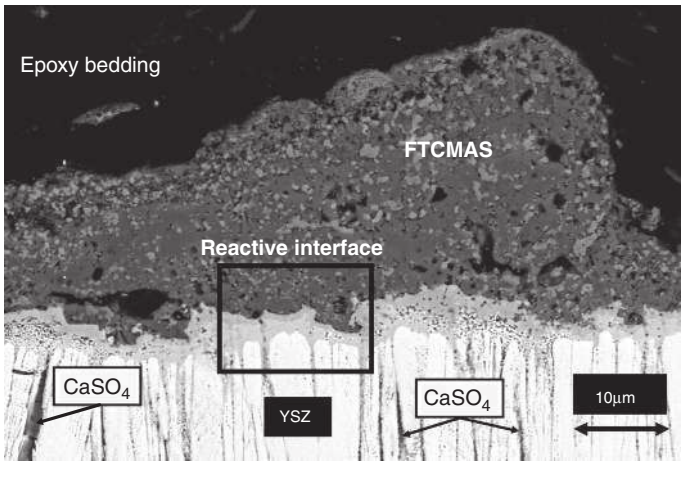

Figure 9.24 Cross-section through the pressure face of the turbine blade shown in **Fig. 9.23**, revealing an adherent CMAS deposit. $CaSO_4$ from the deposit has infiltrated itself along the EB-PVD t-ZrO_2 top coat columnar grain boundaries and attacked its outer surface. Further detail is shown in **Fig. 9.25**.
Courtesy of Wolfgang Brau, Peter Mechnich and Wiley Publications (J. American Ceramic Society). Used with permission. After Brau & Mechnich (2011).

The erosion rate (E) of a material is a dimensionless quantity that can be defined as (Hutchings, 1992):

$$E = \frac{\text{mass of material removed from surface}}{\text{mass of particles striking surface}} \qquad \text{(Equation 9.2)}$$

Sometimes this is expressed, rather pedantically, in units of g/kg (Nicholls et al, 1999) or mg/g (Tabakoff, 1999). The rate of attack of material by erosion varies with the angle of incidence between the particle trajectory and the material surface. When the highest rate of degradation occurs at an angle of incidence of 90°, the material response is defined as 'brittle', whereas if maximum erosion happens at an angle of incidence of 30°, it is defined as 'ductile'. (Also refer to **Section 6.2, Chapter 6**.) This can be slightly misleading. Some ceramic materials can show ductile erosion behaviour; here, the ceramic absorbs or sustains deformation by a mechanism of micro-crushing – where fractures have a short length and *either* do not cause immediate failure *or* only permit the removal of 'small' fragments of material. In contrast, ceramic materials that show brittle erosion behaviour will allow longer fractures to form, leading to the removal of 'large' fragments of material. Both scenarios are depicted in **Fig. 9.26**.

Tabakoff (1999) showed the erosion of diffusion bond coatings like Pt-aluminide to be ductile in character. He observed maximum erosion when these materials were bombarded by fly ash particles (pre-heated to 815°C) propelled at an impingement angle of ~30°, with an impact velocity of 366m/s. The reported erosion values were 10 times *lower* than those of an uncoated nickel alloy substrate, Ni-9Cr-5.5Al-10Co-1.5Ta-1.5Ti-2.4Mo (MAR-M246). Nicholls et al (1999)

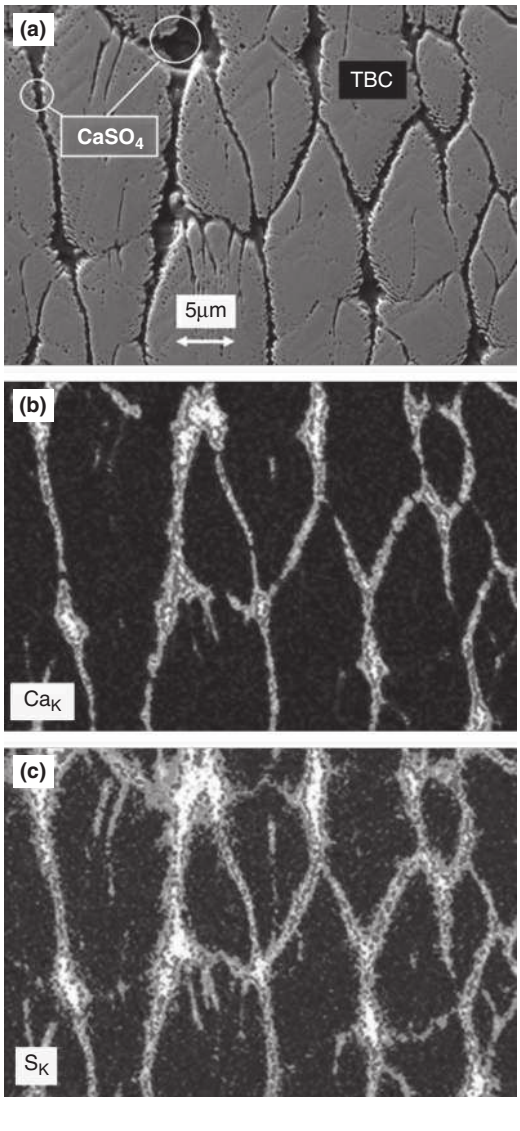

Figure 9.25 Cross-section through the suction face of the turbine blade shown in **Fig. 9.23**, showing the central region of the EB-PVD t-ZrO_2 top coat: (a) secondary electron image; (b) Ca K α X-ray map; (c) SK_α X-ray map. This strongly indicates the penetration of molten $CaSO_4$ along the t-ZrO_2 grain boundaries during operational use.
Courtesy of Wolfgang Brau & Springer Science. Used with permission. After Brau, 2009.

compared the erosion behaviour of an M-Cr-Al-Y overlay bond coat with that of sintered monolithic t-ZrO_2, APS-t-ZrO_2 and EB-PVD t-ZrO_2 when using an impact angle of 90°. These workers used 100μm particles of Al_2O_3 to bombard their test surfaces. In the one experimental set-up, the particles were pre-heated to 910°C and propelled at a velocity of 230m/s; in another, particles were kept at ambient temperature (~20° C), at which they attained a velocity of ~140m/s. Their results (**Fig. 9.27**) indicate that thermal barrier systems having an EB-PVD t-ZrO_2 top coat are more erosion tolerant than those deploying an APS t-ZrO_2 top coat. They also reported maximum erosion attack at an impact angle of 90°; under these conditions, the M-Cr-Al-Y overlay bond coating was more erosion resistant than either t-ZrO_2 variant (**Fig. 9.26**). This is unsurprising since such high-impact angles cause the least erosion for ductile materials (Hutchings, 1992). Of high importance,

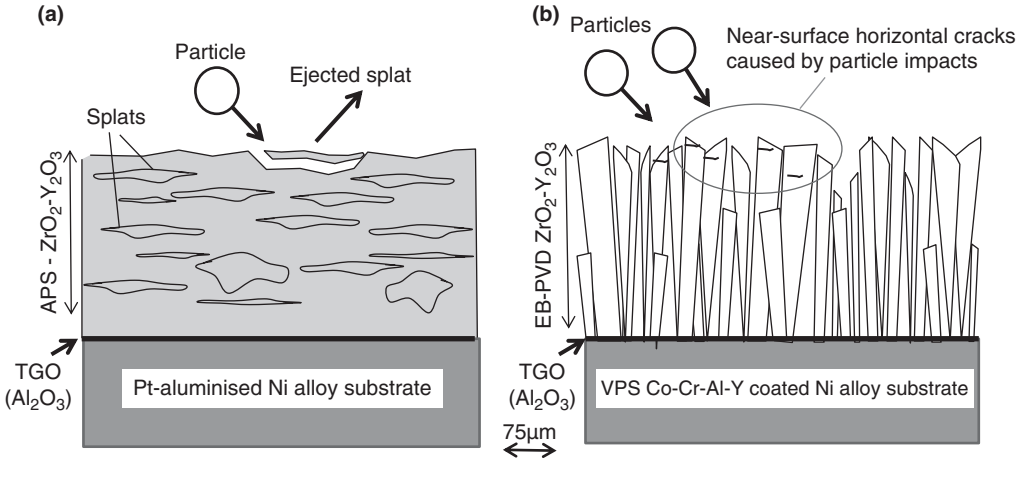

Figure 9.26 Schematic indicating modes of ZrO_2-Y_2O_3 coating fracture during particle erosion of: (a) air plasma–sprayed (APS) coating – failure takes place along splat boundaries; (b) EB-PVD coating – short horizontal cracking across grain columns limited by grain boundaries. Note the substrate (in either case) may be Pt-aluminised or vacuum/shrouded plasma-sprayed Co-Cr-Al-Y. (Coating thicknesses are not to scale.)
Based on an original drawing by Nicholls et al (1999).

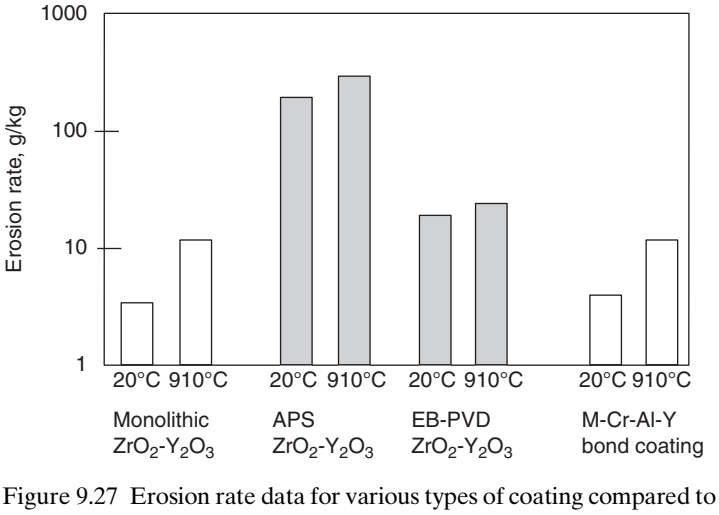

Figure 9.27 Erosion rate data for various types of coating compared to monolithic ZrO_2-Y_2O_3. Eroding particles were ~100µm diameter alumina, made to impact the test surfaces at 90 degrees. Temperatures refer to air temperature used to carry the alumina. Particle velocity at 20°C~ 140m/sec, at 910°C~ 230m/sec.
After Nicholls et al, 1999.

however, was their observation that EB-PVD t-ZrO_2 coatings display erosion-induced fracture within a narrowly confined near-surface region where cracks cannot grow beyond the confinement of their open columnar grain boundaries (**Fig. 9.26b**). In the case of APS-deposited t-ZrO_2, however, crack lengths are much larger (for a given impacting particle force), as these defects are able to propagate

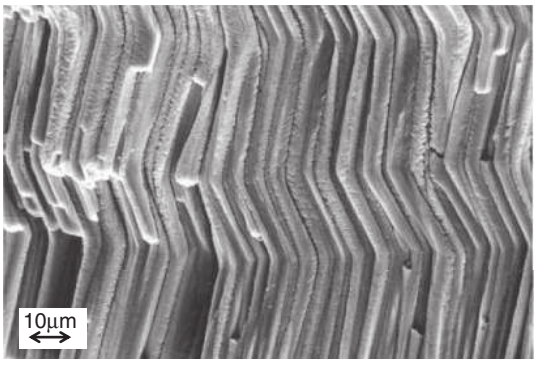

Figure 9.28 Wavy (herringbone or zigzag) structured EB-PVD t-ZrO_2 thermal barrier top coat.
After Schulz et al, 2004. © Wiley, 2004. Used with permission.

along inter-splat boundaries (**Fig. 9.26a**). This causes larger fragments of coating material to be removed compared to EB-PVD t-ZrO_2, where crack lengths are shorter. Accordingly, a significantly higher rate of erosion of APS-deposited t-ZrO_2 takes place (**Fig. 9.27**).

In a bid to develop alternatives to the present-day reliance on TBCS using EB-PVD t-ZrO_2 top coats like that shown in **Fig. 9.20**, one major company, GE, has evaluated the erosion and impact resistance of more than two hundred alternative compositional and microstructural variants (Darolia, 2013) – an effort that was, unfortunately, unsuccessful. However, one interesting finding, based on field test results, was that turbine section blades fitted with a novel external EB-PVD t-ZrO_2 coating with a 'herringbone' or zigzag columnar patterned grain structure (US Patent 7,318,955) – e.g., see **Fig. 9.28** – showed better damage tolerance against particle erosion than conventional vertically aligned, columnar t-ZrO_2 top coats. The wavy grain structure had the effect of limiting fracture growth to planes parallel to, but at significant distance from, the EB-PVD t-ZrO_2/TGO interface, reducing the amount of material that could be removed following a given quantity of particle bombardment. However, some workers disagree with this inference (Schulz et al, 2004) and report a lowering of erosion resistance when using herringbone-structured t-ZrO_2 coatings. In the same review, the same structures are claimed to lower thermal conductivity; in principle, this would further reduce heat flow through the ZrO_2 component of the thermal barrier coating system. However, at the time of writing, the extent of uptake of the herringbone-structured top coat design (**Fig. 9.28**), relative to conventional straight-columned t-ZrO_2 coatings (**Fig. 9.22a**), is unknown.

Doping t-ZrO_2 with small concentrations (2–5wt-%) of rare earths (such as the oxides of Dy and Gd) can have the beneficial effect of reducing the thermal conductivity (K) and, coincidently, also make them more resistant to CMAS attack. However, particle impact tests on such materials (Wellman & Nicholls, 2007; Ndamka, 2013) have shown a worsening in erosion resistance. Hence, up to the time of writing, the challenge remains in place to develop new and improved TBCS materials and designs.

References

Booth, G. C. and Clarke, R. L. (1986), 'Evaluation of corrosion resistance of coated superalloys in rig tests', *Materials Science & Technology* **2**, 272–281.

Boyce, M. P. (2012), *Gas turbine engineering handbook*, 4th edn, Butterworth-Heinemann, Oxford, 401–425 and 509–514.

Brau, W. (2009), 'Environmental stability of the YSZ layer and the YSZ/TGO interface of an in-service EB-PVD coated high pressure turbine blade', *Journal of Materials Science* **44**, 1664–1675.

Brau, W. and Mechnich, P. (2011), 'Recession of an EB-PVD YSZ coated turbine blade by $CaSO_4$ and Fe, Ti rich CMAS-type deposits', *Journal of the American Ceramic Society* **94** (12), 4483–4489.

Bürgel, R. (1986), 'Coating service experience with industrial gas turbines', *Materials Science & Technology* **2**, 302–308.

Cetel, A. D. and Duhl, D. N. (1988), 'Second generation nickel base single crystal superalloy', in *Superalloys TMS*, Minerals, Metals & Materials Society.

Condé, J. F. G., Booth, G. C. and Taylor, A. F. (1986), 'Protection against hot corrosion in marine gas turbines', *Materials Science & Technology* **2**, 314–317.

Darolia, R. (2013), 'Thermal barrier coatings technology: Critical review, progress update, remaining challenges and prospects', *International Materials Reviews* **58** (6), 315–248.

de Wet, D. J., Stott, F. H. and Taylor, R. (1993), 'The degradation of ZrO2-Y2O3 thermal barrier coatings by molten middle east sand', *Surface Engineering, Volume II: Engineering Applications* (based on the proceedings of the 3rd international conference on advances in coatings and surface engineering for corrosion and wear resistance), Royal Society of Chemistry, London, 210–219.

Fitzer, F. and Schlichting, J. (1983), 'Coatings containing chromium, aluminium and silicon for high temperature alloys', in *High temperature corrosion*, National Association of Corrosion Engineers (NACE), Houston, Texas, 604–614, edited by R. A. Rapp.

Goward, G. W. (1983), 'Recent developments on high temperature coatings for gas turbine airfoils', in *High temperature corrosion*, National Association of Corrosion Engineers (NACE), Houston, Texas, 553–560, edited by R. A. Rapp.

Goward, G. W. (1986), 'Protective coatings – Purpose, role, and design', *Materials Science & Technology* **2**, 194–200.

Goward, G. W. (1998), 'Progress in coatings for gas turbine airfoils', *Surface Coatings & Technology* **108–109**, 73–79.

Grindle, T. J. and Burcham, F. W. (2003), 'Engine damage to a NASA DC-8-72 airplane from a high altitude encounter with a diffuse volcanic ash cloud', NASA Report TM-2003-212030.

Han, J. C., and Wright, L. M. (2007), 'Enhanced internal cooling of turbine blade and vanes,' *The gas turbine handbook – U.S. DOE*, National Energy Technology Laboratory, Morganton, USA, section 4-2-2-2, 321–35.

Hancock, P. (1986), 'Future direction of research on high temperature coatings', *Materials Science & Technology* **2**, 310–313.

Harris and Wahl (2004), 'Improved single crystal superalloys, CMSX-4 (SLS)[La+Y] and CMSX-486', in *Superalloys 2004*, TMS (The Minerals, Metals & Materials Society), edited by K. A. Green, T. M. Pollock and H. Harada.

Harry, N. J. V. (1986), 'Marine applications', *Materials Science & Technology* **2**, 295–301.

Hutchings, I. J. (1992), '*Tribology – Friction and wear of engineering materials*', Edward Arnold, London, 172–182.

Jordon, H. (and 9 others), (2004), 'Superior thermal barrier coatings using solution precursor plasma spray', *Journal of Thermal Spray Technology* **13** (1), 57–65.

Kaden, U., Leyens, C., Peters, M. and Kaysser, W. A. (1999), 'Thermal stability of an EB-PVD thermal barrier coating system on a single crystal nickel base superalloy', in *Elevated*

temperature coatings: Science & Technology III, The Metals & Minerals Society, 27–38, edited by J. M. Hampikian and N. B. Dahotre.

Kircher, I. A., Mordie, B. G. and McCarter, A. (1994), 'Performance of silicon modified aluminide coating in high temperature hot corrosion test conditions', *Surface and Coatings Technology* **68/69**, 32–37.

Leyens, C., Wright, I. G. and Pint, B. A. (1999), 'Hot corrosion of nickel base alloys in biomass derived fuel simulated atmosphere', in *Elevated temperature coatings: Science & Technology III*, The Metals & Minerals Society, 79–90, edited by J. M. Hampikian and N. B. Dahotre.

Lotrakul, P., Trice, R. W., Trumble, K. P. and Dayananda, M. A. (2014), 'Investigation of the mechanisms of Type-II hot corrosion of superalloy CMSX-4', *Corrosion Science* **80**, 408–415.

Meetham, G. W. (1986), 'Use of protective coatings in aero gas turbine engines', *Materials Science & Technology* **2**, 290–294.

Ndamka, N. L. (2013), 'Microstructural damage of thermal barrier coatings due to CMAS attack', PhD thesis, Cranfield University, UK.

Ndamka, N. L. (2014), 'Turbine blade coatings feel the heat', Materials World, April, 30–33.

Nicholls, J. R., Deakin, M. J. and Rickerby, D. S. (1999), 'A comparison between the erosion behaviour of thermal spray and electron beam physical vapour deposition thermal barrier coatings', *Wear* **233–235**, 352–361.

Nicholls, J. R., Simms, N. J., Chan, W. Y. and Evans, H. E. (2002), 'Smart overlay coatings – Concept and practice', *Surface and Coatings Technology* **149** (2–3), 236–244.

Nicoll, A. R. (1982), 'Self fluxing coatings for stationary gas turbines', *Thin Solid Films* **95** (3), 285–295.

Pettit, F. (2011), 'Hot corrosion of metals and alloys', *Oxidation of Metals* **76**, 1–21.

Rapp, R. A. (2002), 'Hot corrosion of materials: A fluxing mechanism?' *Corrosion Science* **44**, 209–221.

Saunders, S. R. J. (1986), 'Correlation between laboratory and corrosion rig testing and service experience', *Materials Science & Technology* **2**, 282–289.

Saunders, S. R. J. and Nicholls, J. R. (1984), 'Hot salt corrosion test procedures and coating evaluation', *Thin Solid Films* **119**, 247–269.

Saunders, S. R. J. and Nicholls, J. R. (1989), 'Coatings and surface treatments for high temperature oxidation resistance', *Materials Science & Technology* **5**, 780–798.

Schulz, U., Saruhan, B., Fritscher, K. and Leyens, C. (2004), 'Review of advanced EB-PVD ceramic topcoats for TBC applications', *International Journal of Applied Creamic Technology* **1** (4), 302–315.

Smith, A. B., Kempster, A. and Smith, J. (2000), *Characterisation of aluminide coatings formed on nickel-base superalloys by vapour aluminising*, IOM Communications, London, 13–27.

Tabakoff, W. (1999), 'Erosion resistance of superalloys and different coatings exposed to particulate flows at high temperature', *Surface & Coating Technology* **120–121**, 542–547.

Tamarin, Y. (2006), *Protective coatings for turbine blades*, ASM International, Materials Park, Ohio, USA, 25–34.

Vialas, N. and Monceau, D. (2006), 'Substrate effect on high temperature oxidation of Pt modified aluminide coating Part 1', *Oxidation of Metals* **66** (3/4), 155–189.

Wellman, R. G. and Nicholls, J. R. (2007), 'A review of the erosion of thermal barrier coatings', *Journal of Physics D: Applied Physics* **40**, R293–R305.

Wu, W. T., Rahmel, A. and Schorr, M. (1983), 'Acidic and basic fluxing of Ni-base superalloys in a $90Na_2SO_4$–$10K_2SO_4$ melt at 1173 K', *Oxidation of Metals* **19** (5/6), 201–229.

Wu, W. T., Rahmel, A. and Schorr, M. (1984), 'Role of platinum in the Na_2SO_4 induced hot corrosion resistance of aluminium diffusion coatings', *Oxidation of Metals* **22** (1/2), 59–81.